The Intrinsic Communication in Power Systems: A New Perspective to Understand Synchronization Stability

Yitong Li, *Member, IEEE*, Timothy C. Green, *Fellow, IEEE*, Yunjie Gu, *Senior Member, IEEE*

***Abstract*—The large-scale integration of converter-interfaced resources in electrical power systems raises new threats to stability which call for a new theoretical framework for modelling and analysis. In this paper, we present the intrinsic analogy of a power system to a communication system, which is here called power-communication isomorphism. Based on this isomorphism, we revisit power system stability from a communication perspective and thereby establish a theory that unifies the heterogeneous power apparatuses of power systems and provides a bridge between electromagnetic transient (EMT) and phasor dynamics. This theory yields several new insights into power system stability and new possibilities for stabilization. In particular, we demonstrate that a system of 100% converter-interfaced resources can achieve stable synchronization in small- and large-signal sense under grid-following control which was commonly considered impossible.**

***Index Terms*—Power-communication isomorphism, synchronization, stability, dynamics, power systems, channel.**

I. Introduction

Driven by the imperative of decarbonisation and clean growth, the primary energy of electric power systems is transforming from fossil fuels to renewable resources. The change of the primary energy is accompanied by a change of technologies for power generation and conversion. Renewable resources, mainly wind and solar energy, as well as grid-scale battery storage plants, are interfaced to power systems by power electronic converters instead of conventional synchronous generators. The increasing penetration of converter-interfaced resources poses new threats to system stability [1]. Converter-induced oscillations have been reported worldwide, many of which had major consequences. For example, the 2019 power outage in UK was, in part, triggered by a sub-synchronous oscillation of wind turbine converters in Hornsea windfarm according to the report provided by National Grid UK [2]. The underpinning mechanisms of power system stability are not fully understood and this has drawn international attention.

The stability of a power system is defined as the ability to keep all apparatus in the system synchronized to a single frequency with power flows and voltage profiles throughout the system within some expected range [3], [4]. The classic synchronization stability theory for power systems is tailor-made for synchronous generators which are govern by the physical law of the motion of their rotors. However, converters are governed by control algorithms, which gives increased flexibility, and therefore complexity, in converter behaviours [5], [6]. Up to now, the control-defined behaviour of converters are categorised into two classes. The first class, called grid-forming [6]–[9], behaves as a voltage source which synchronizes to the grid according to power balancing, such as synchronous generators, grid-forming converters, etc. The second class, called grid-following [6], [10]–[14], behaves as a current source (or sink) which synchronizes to the grid according to voltage signals and phase-locked loops (PLLs), such as grid-following converters. This forming-following dichotomy creates a heterogeneous grid that sets a barrier for whole-system synchronization stability analysis [6], [15], [16].

To address the aforementioned challenges, we looked again at the nature of synchronization in ac electric power systems. We investigate the analogy between power systems and communication systems by comparing power apparatuses to communication modulators and comparing power networks to communication channels. This analogy is formalised as a concept of *power-communication isomorphism*. Via this isomorphism, information on phase angles is embedded within power and propagated along a power network via an equivalent modulation-demodulation process, which explains why power systems are capable of "self-synchronizing". The isomorphism also describes how heterogeneous grid-forming and grid-following apparatuses can be unified into a general synchronization model. We further illustrate that the electromagnetic transient (EMT) of power networks can be represented as a communication channel, and we use concepts of "dynamic frequency shift" and "channel bandwidth" to illuminate how EMT dynamics interact with phasor dynamics, inspired by the relationships between the carrier-band and base-band signals in communication. The communication channel can well represent all passive electrical elements (transmission lines, transformers, machine windings, and shunt/series compensators), as well as the virtual passive elements equivalent to the inner control loops of converters [17]. Using these new insights from the communication perspective, we revisited power system stability which gives rise to many interesting new findings: i) the dynamic frequency shift of channels introduces negative damping in synchronization dynamics which can be mitigated

This work was supported by the Xi'an Jiaotong University under Grant 010400-71211222110703, and the Engineering and Physical Sciences Research Council of UK (EPSRC) under Grants EP/T021780/1 and EP/S000909/1. *(Corresponding Author: Yunjie Gu.)*

Yitong Li is with the School of Electrical Engineering, Xi'an Jiaotong University, Xi'an 710049, China (e-mail: yitongli@xjtu.edu.cn).

Timothy C. Green and Yunjie Gu are with the Department of Electrical and Electronic Engineering, Imperial College, London SW7 2AZ, UK. (e-mail: t.green@imperial.ac.uk; yunjie.gu@imperial.ac.uk).

by extra damping control; ii) the channel bandwidth sets the limit speed for power transfer and angle synchronization along power networks, which determines the minimum value of local energy buffer or inertia; iii) grid-following converters see higher channel bandwidths (which means lower necessary energy buffers) than grid-forming converters since inner loops reshapes channel dynamics; iv) grid-following converters synchronize to the grid via a "reactive rotor" (Q-Rotor) in duality to the "active rotor" (P-Rotor) of a grid-forming apparatus. Based on these new findings, we present a case where a power system with nearly 100% grid-following converters can maintain stable synchronization over various transients with a slight modification of the conventional grid-following control. This was commonly considered impossible in state-of-the-art theories and is a useful new result of the new theory.

The rest part of the paper is organised as follows. The concept of power-communication isomorphism is introduced in Section II. Power apparatuses and their outer-loop control are recast as modulators and demodulators in Section III. Power networks and the inner-loop control of converters are recast as communication channels in Section IV. Based on these new perspectives, Section V revisits the synchronization stability in power systems and discuss the new findings. Section VI present a case study on a modified IEEE 68-bus system and illustrate how a system with nearly 100% grid-following converters can maintain stability. Section VII concludes this article.

II. Power-Communication Isomorphism

The concept of power-communication isomorphism is illustrated in Fig. 1. The voltages and currents in a power system are viewed as communication signals carrying both energy and information. The power apparatuses, including generators and converters, serve as modulators in that they create three-phase sinusoidal signals from internal oscillators (rotors, controllers, etc). The amplitude, frequency and phase of an internal oscillator are base-band signals which are shifted to the carrier-band of 50 Hz or 60 Hz via frame transformation or rotation, creating an effect equivalent to amplitude and angle modulation. Mathematically, a three-phase signal is represented as a complex number $Ae^{j\theta}$, where A and θ are the amplitude and angle of the signal [18]–[21]. The amplitude and angle can be combined into a complex phase defined as $\vartheta = \ln A + j\theta$, so the amplitude-angle modulation is jointly expressed as a complex exponential function

$$e^{\vartheta} = Ae^{j\theta} = A(\sin\theta + j\cos\theta) \tag{1}$$

The time-derivative of the ϑ is called the complex frequency $\varpi = \dot{\vartheta} = A^{-1}\dot{A} + j\omega$, whose real part reflects amplitude variation, and the imaginary part $\omega = \dot{\theta}$ is the angular frequency.

The modulated signals are propagated over a power network and that network can be viewed as a set of communication channels. The channels include all passive components in the power network, including transmission lines, transformers, series/shunt compensators, harmonic filters, and passive loads. The inner control loops of converters can be represented as equivalent impedances in series or shunt with the sources, and therefore can also be counted among the channels. The active apparatuses, including generators and converters, are defined as nodes that interact (communicate) over the channels. There are two types of nodes in a power system. A voltage node applies a voltage source to the network, and represents grid-forming apparatuses, including synchronous generators and grid-forming converters [6]. A current node applies a current source to the network, and represents grid-following converters [5], [6], [22]. From the communication point of view, a voltage node transmits a voltage signal to the network and receives a current signal, and a current node does the opposite. There may be multiple nodes in the network and their signals are received at each node as a single signal by superposition. The complex power seen at a node is defined as [23]

$$S = e^{\vartheta_{\text{rx}}} e^{\vartheta_{\text{tx}}^{\star}} = A_{\text{tx}} A_{\text{rx}}\, e^{j(\theta_{\text{rx}} - \theta_{\text{tx}})} \tag{2}$$

where $e^{\vartheta_{\text{tx}}}$ is the transmitted signal, $e^{\vartheta_{\text{rx}}}$ is the received signal, and the superscript * denotes complex conjugation. It is worth noting that, $A_{\text{rx}}e^{\theta_{\text{rx}}}$ and $A_{\text{tx}}e^{\theta_{\text{tx}}}$ are ac signals, but S can be dc at steady-state if $\omega_{\text{rx}} = \dot{\theta}_{\text{rx}}$ equals to $\omega_{\text{tx}} = \dot{\theta}_{\text{tx}}$ and $\theta_{\text{rx}} - \theta_{\text{tx}}$ is constant. In other words, the complex power has a demodulation effect that converts a carrier-band signal to base-band.

III. Power Apparatuses versus Modulators

Synchronization is an essential element for all power apparatuses in ac power grids. There are heterogeneous synchronization schemes co-existing in power systems which present an obstacle to systemic analysis. Voltage nodes use power-based synchronization via physical or emulated rotors [6], [24], [25], whereas current nodes use signal-based synchronization via phase-locked loops (PLLs) [6], [26]. The theory of power-communication isomorphism illuminates the unified synchronization principle underlying the power- and signal-based synchronization schemes.

The essence of synchronization is to detect the angle difference between nodes and mitigate the difference via feedback control of the frequency of the oscillators of the nodes in question. In the light of power-communication isomorphism, the demodulated complex power S is a natural candidate for angle detectors. However, S is a complex number, so its real and imaginary parts are used in practice. For a voltage node, the active power $P = \text{Re}(S)$ is used as an angle detector; for a current node, the q-axis voltage $v_q = \text{Im}(v_{dq})$ is used as an angle detector. It is worth noticing that $P = i_d A_v \propto i_d$ and $Q = v_q A_i \propto v_q$, which implies the power calculation is equivalent to the dq-frame signal transformation. This establishes the equivalence of the power-based and signal-based synchronization with a unified synchronization principle, as illustrated in Fig. 2. The rotor of a voltage node is equivalent to a PLL synchronizing to the current i_d, and the PLL of a current node is equivalent to a rotor accelerating/decelerating under reactive power Q when i_q is zero. This gives the duality relationship between the synchronization of voltage and current nodes [6].

The discussion above on $Q = v_q A_i \propto v_q$ is based on the assumption that $i_q = 0$ which may not always hold. To address

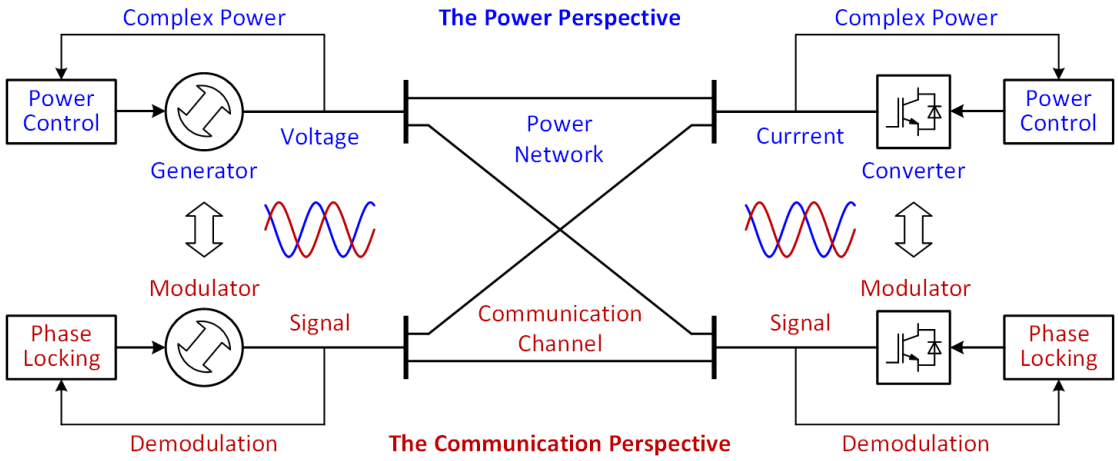

Fig. 1. Illustration of power-communication isomorphism in power systems. The upper part shows a part of system viewed from the perspective of power transfer and the lower part is viewed from the perspective of communication.

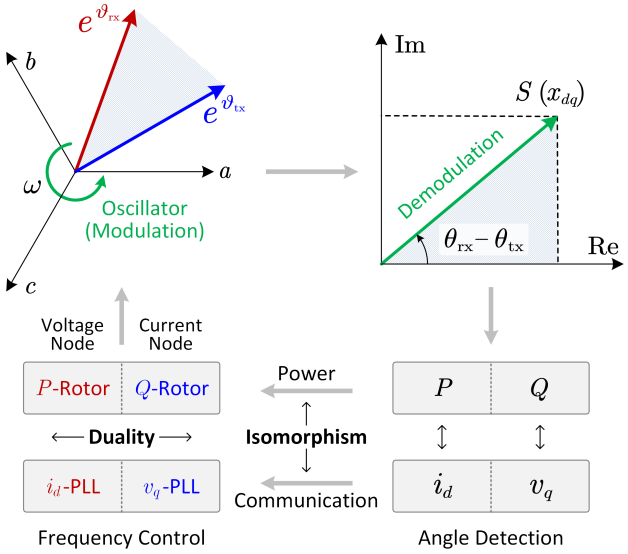

Fig. 2. Unified synchronization principle in the light of power-communication isomorphism: the equivalence of rotor and PLL, and the duality of voltage and current nodes. We use a prefix to distinguish the conventional rotor and PLL (P-Rotor, v_q-PLL) and the ones derived from the isomorphism (Q-Rotor, i_d-PLL).

this, we introduce the generalized power W. Angle detection via P and Q can be generalized by introducing an angle μ on which the complex power S is projected

$$W = \mathrm{Re}(e^{-j\mu}\, S) \tag{3}$$

where W is named *generalized power*, and the associated frequency control is governed by a *generalized rotor*. If μ is set to 0 or $\pi/2$, W is P or Q respectively. For a current node with $i_q \neq 0$, we set the projection angle to be the complementary power factor angle, that is $\mu = \pi/2 - \mathrm{atan}(i_q/i_d)$, so that $W \propto v_q$ serves as the angle detector. The projection angle μ can be set to other values which yields new synchronization methods in the middle ground between the forming-following dichotomy. The synchronization dynamics of associated to W is

$$H\dot{\omega} = W^* - W - D\omega \tag{4}$$

where H is generalised inertia, D is generalised damping, and W^* is *generalized power reference*. This equation unifies the synchronization dynamics of all apparatuses in power systems. The mathematical details of the generalised synchronisation principle is elaborated in detail in Appendix A.

IV. Power Networks versus Communication Channels

In a communication system, the dynamics of a communication channel determine the maximum communication rates according to the Shannon-Hartley theorem [27], [28]. In this section, we investigate the role of channel dynamics in power systems.

A. Mathematical Formulation

We use g_{mn} to represent the channel gain when a signal (current or voltage) is transmitted from node n to node m. By varying m and n, we can get a channel gain matrix $[g]$, which reflects the communication topology of the network. On the other hand, the dynamic nodal admittance matrix $[Y]$ defines the power (physical) topology of the network [3], [29], where the "dynamic" means $[Y]$ is a transfer function matrix [29] rather than a complex-value nodal admittance matrix conventionally used in power flow analysis [3]. We show how the communication and power topology are related next.

Suppose that the voltage nodes in the network are numbered by $\{1, 2, \cdots, N_v\}$ and current nodes by $\{N_v+1, N_v+2, \cdots, N_v+N_i\}$, where N_v and N_i are the total number of voltage and current nodes respectively. We partition $[Y]$ at the N_v-th row and N_v-th column:

$$[Y] = \begin{bmatrix} [Y_{vv}] & [Y_{vi}] \\ [Y_{iv}] & [Y_{ii}] \end{bmatrix} \tag{5}$$

and we have

$$\begin{aligned} [i_v] &= [Y_{vv}][v_v] + [Y_{vi}][v_i] \\ [i_i] &= [Y_{iv}][v_v] + [Y_{ii}][v_i] \end{aligned} \tag{6}$$

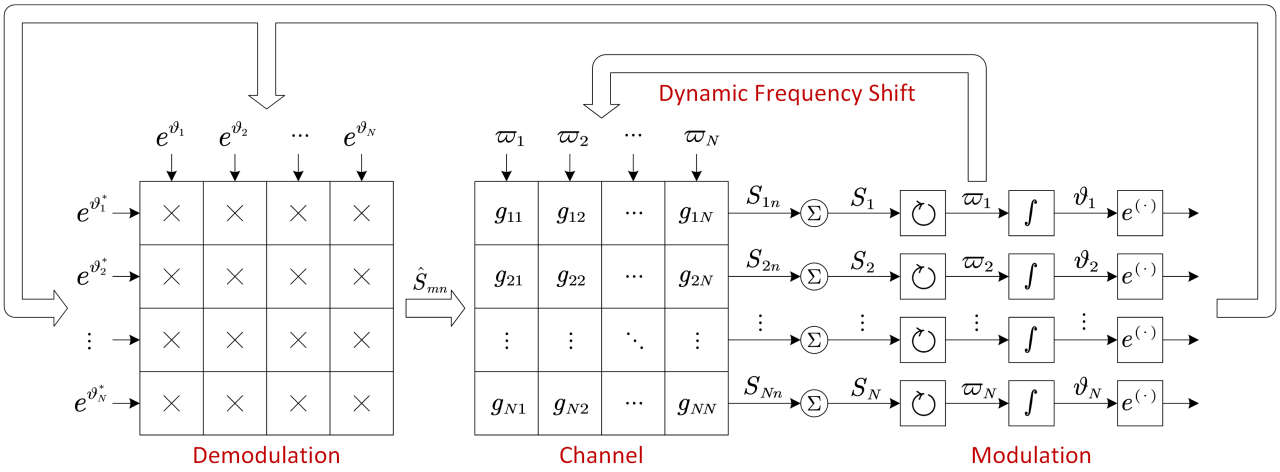

Fig. 3. The overall model of the power-communication isomorphic system considering the dynamic channel gains. Symbols: $*$ denotes complex conjugation, $\times$ denotes multiplication, $\sum$ denotes summation, $\int$ denotes integration, and $\circlearrowleft$ denotes the oscillator that synthesises the internal complex frequency according to the balancing of the complex power.

where $[v_v]$ and $[v_i]$ are vectors representing the voltages at the voltage and current nodes respectively, and $[i_v]$ and $[i_i]$ are the corresponding current vectors. From the communication perspective, $[v_v]$ and $[i_i]$ are transmitted by nodes, and $[i_v]$ and $[v_i]$ are received from the network. Thus we rearrange (6) to show the mapping from $[v_v, i_i]$ to $[i_v, v_i]$

$$\begin{aligned}[i_v] &= \left([Y_{vv}] - [Y_{vi}][Y_{ii}]^{-1}[Y_{iv}]\right)[v_v] + [Y_{vi}][Y_{ii}]^{-1}[i_i] \\ [v_i] &= -[Y_{ii}]^{-1}[Y_{iv}][v_v] + [Y_{ii}]^{-1}[i_i]\end{aligned} \tag{7}$$

from which follows

$$[g] = \begin{bmatrix} [Y_{vv}] - [Y_{vi}][Y_{ii}]^{-1}[Y_{iv}] & [Y_{vi}][Y_{ii}]^{-1} \\ -[Y_{ii}]^{-1}[Y_{iv}] & [Y_{ii}]^{-1} \end{bmatrix}. \tag{8}$$

i.e., the channel gain matrix. If the network only contains voltage nodes, $[g] = [Y]$, indicating that the communication and power topology are identical. Otherwise, the power topology $[Y]$ is twisted in the communication topology $[g]$ due to the interaction of current and voltage nodes.

B. Dynamic Frequency Shift

A channel (e.g., a transmission line) consists of linear circuits and therefore can be represented as a linear transfer function $G(s)$ in frequency domain. Since the modulation-demodulation has a frequency shifting effect, the equivalent transfer function seen by the base-band signals is shifted to $G(j\omega_c + s)$ according to Fourier analysis [28]. This frequency shift representation assumes a constant carrier frequency which does not hold for a power system where different nodes may have different instantaneous carrier frequencies that are varying in real-time subject to load balancing. To address this issue, we propose a new time-domain representation for a channel. The time-domain gain of a channel is defined as $g = e^{\vartheta'}/e^{\vartheta}$ where e^{ϑ} and $e^{\vartheta'}$ are the input and output signals of the channel respectively. The alternating part of e^{ϑ} and $e^{\vartheta'}$ are cancelled in the division so g is a base-band variable. $G(s)$ can be decomposed into a series of first-order systems $G(s) = \sum_k (s - p_k)^{-1} a_k$, each of which induces a gain g_k, and the total gain is the sum of all g_k. We simply investigate one of the first-order systems $G(s) = (s-p)^{-1}a$ without losing generality, where p is the pole of $G(s)$ and a is the coefficient. The corresponding differential equation for the signal passing the channel is

$$d\, e^{\vartheta'}/dt = p\, e^{\vartheta'} + a\, e^{\vartheta} \tag{9}$$

which yields the differential equation for the channel gain g

$$dg/dt = (p - \varpi)g + a. \tag{10}$$

It is clear that g depends on ϖ dynamically, and this effect is named *dynamic frequency shift* as an extension to the (static) frequency shift in Fourier analysis.

Taking into account the dynamic channel gain, the overall model for the power-communication isomorphic system is illustrated in Fig. 3. For a network with N nodes, the n-th node transmits a signal e^{ϑ_n} to the network which is demodulated by another node m to yield $\hat{S}_{mn} = e^{\vartheta_n} e^{\vartheta_m^*}$. We put $\hat{}$ on $\hat{S}_{mn}$ because it is not physical power as the channel gain is not yet included. Considering the channel gain, the complex power transfer over the channel from the n-th node to the m-th node is $S_{mn} = g_{mn}\hat{S}_{mn}$ where g_{mn} is the corresponding channel gain. All traffic in the network shares the channels according to the superposition principle, so the total complex power received at node m is the summation: $S_m = \sum_n S_{mn}$ [1]. The total complex power S_m is fed to the oscillator of the m-th node. The oscillator governs the complex frequency ϖ_m which is integrated to the complex angle ϑ_m. The signal e^{ϑ_m} is modulated from ϑ_m and transmitted to channels, and thus closes the loop of modulation-demodulation.

C. Channel Bandwidth

The dynamic frequency shift illuminates interesting properties of base-band signal propagation over a channel. To

[1]For example, for a two-bus system, the total complex power at bus 1 is $S_1 = S_{11} + S_{12}$. Just be careful that S_{11} should also be considered to get the total complex power, based on the superposition theorem.

illustrate this, we find the linearized solution of g from (10) and put it into S_{mn}

$$\Delta S_{mn} = S_{mn0}(\Delta\vartheta_m^* + F\cdot\Delta\vartheta_n) \tag{11}$$

where the prefix Δ and subscript 0 denote the perturbation and equilibrium of a dynamic variable, and F is a low pass filter

$$F(s) = \frac{j\omega_0 - p}{s + j\omega_0 - p}. \tag{12}$$

The detailed derivation of (11) and (12) can be found in Appendix C. It is clear from (11) that a channel induces asymmetry in base-band signal propagation. The angle perturbation $\Delta\vartheta_m$ at the receiving end m affects the complex power ΔS_{mn} instantaneously, whereas the angle perturbation $\Delta\vartheta_n$ at the transmitting end n passes through a low-pass filter F before affecting ΔS_{mn} [2]. Thus we defined the *channel bandwidth* as

$$\begin{gathered}\omega_{\mathrm{b}} = \sup|\omega|, \text{ subject to} \\ |F(j\omega)| > 1/\sqrt{2} \text{ and } |\angle F(j\omega)| < \pi/4.\end{gathered} \tag{13}$$

The channel bandwidth identifies the limit speed of power transfer and angle synchronization on the channel. Within the channel bandwidth, the dynamic channel gain g responds almost instantaneously to ϖ. In such a case, g can be approximated by letting $dg/dt = 0$ in (10) which yields

$$g \approx (\varpi - p)^{-1}a = G(\varpi). \tag{14}$$

The base-band signals are equivalent to phasors, and the channel dynamics are equivalent to EMTs in power systems. For example, an inductive line is modelled as $j\omega_0 L = jX$ in phasor-domain analysis, where X is a steady-state reactance, i.e., a constant value. By contrast, the same inductive line is modelled as $j\omega L$ where ω is variable in EMT analysis [3]. In other words, if we set $g_{mn} = G(\varpi_0)$ which gives phasor-domain steady-state channel network, and if we set $g_{mn} = G(\varpi_n)$ which includes the dynamics from ϖ_n to channel and therefore the so-called EMT channel dynamics.

The channel bandwidths in power systems are well below the switching frequency of converters due to the effect of filters and other components with filtering effects. This implies that switching harmonics do not propagate over the channels and their effects in affecting synchronisation can be neglected.

Another concern is that a converter normally has internal circuits and inner-loop controllers, such as LCL filters, current controllers of grid-following converters, and voltage controllers of grid-forming converters. These elements can all be modeled as part of the channel by recasting inner-loop control as linear virtual circuit elements in shunt or series connection with the converter [17]. A brief overview of the circuit representations for the inner control loops of grid-forming and grid-following converters is presented in Appendix B. As a result, the impacts of the inner control loops on synchronisation stability can be reflected by their reshaping the channel bandwidth of power networks.

[2]Just be careful that ΔS_{mn} with $n = m$ also satisfies (11), i.e., $\Delta S_{mm} = S_{mm0}(\Delta\vartheta_m^* + F\cdot\Delta\vartheta_m)$. This gives the self-complex power at bus m.

V. Rethinking Synchronization Stability of Power Systems

The power-communication isomorphism theory provides a new perspective to rethink power system synchronization stability, as elaborated next.

A. Power Control Speed and Channel Bandwidth

The channel bandwidth determines the maximum speed of power transfer and angle synchronization over the network. The channel bandwidth ω_{b} is determined by the pole of the channel. There are four types of channels in a network, namely voltage-voltage, voltage-current, current-voltage, current-current channels. A voltage-voltage channel is the channel between two voltage nodes, and other types are defined similarly. A voltage-voltage channel is generally an inductive transmission line with a very small resistance, so its pole is approximately zero and the corresponding channel bandwidth is $0.41\omega_0$ (ω_0 is 50 or 60 Hz). Other channels where current nodes are associated (i.e., voltage-current, current-voltage, and current-current channels) have a negative-real pole so their channel bandwidths are higher, as marked in Fig. 4 (a). This is because the parallel connected passive loads and the current control loops induce equivalent shunt resistances at the current node which damps the channel pole. Due to the different channel bandwidths, a voltage node normally has a low power control speed (e.g., large inertia of synchronous generators) and current node normally has a high power control speed (e.g., fast current and power control of grid-following converters) in practice. This also results in high transient power and energy perturbation of voltage node [see Fig. 4 (b)], and low transient power and energy perturbation of current node [see Fig. 4 (c)].

B. Synchronization Damping and Dynamic Frequency Shift

Combining the synchronization principle in (3) and (4), with the channel model in (2) and Fig. 1, we get the dynamic model for the mth arbitrary apparatus with considering whole-system interactions as

$$H_m\dot{\omega}_m = W_m^\star - W_m - D_m\omega_m \tag{15}$$

with

$$W_m = \mathrm{Re}\left(e^{-j\mu_m}\textstyle\sum_n g_{mn}A_mA_ne^{-(\theta_m-\theta_n)}\right) \tag{16}$$

W_m depends on θ_m and θ_n which gives the synchronizing coefficient as discussed later in next subsection. Here, according to (14), the channel gain $g_{mn} \approx G_{mn}(j\omega_n)$ is a function of ω_n, i.e., the dynamic frequency shift of channels. This means W_m also depends on ω_n. $\partial W_m/\partial\omega_n$ tends to induces negative damping. For example, for a synchronous generator, $\partial W/\partial\omega = \partial P/\partial\omega = \partial(V_1V_2\sin(\Delta\theta)/\omega L)/\partial\omega < 0$. This negative damping is essentially introduced by the frequency-dependent line inductor ωL in EMT analysis, compared to the phasor analysis with assuming a constant $\omega_0 L = X$. This negative damping would lead to system instability if the damping D_m of the apparatus itself is not sufficiently large. Fig. 5 shows the test result of a synchronous generator with

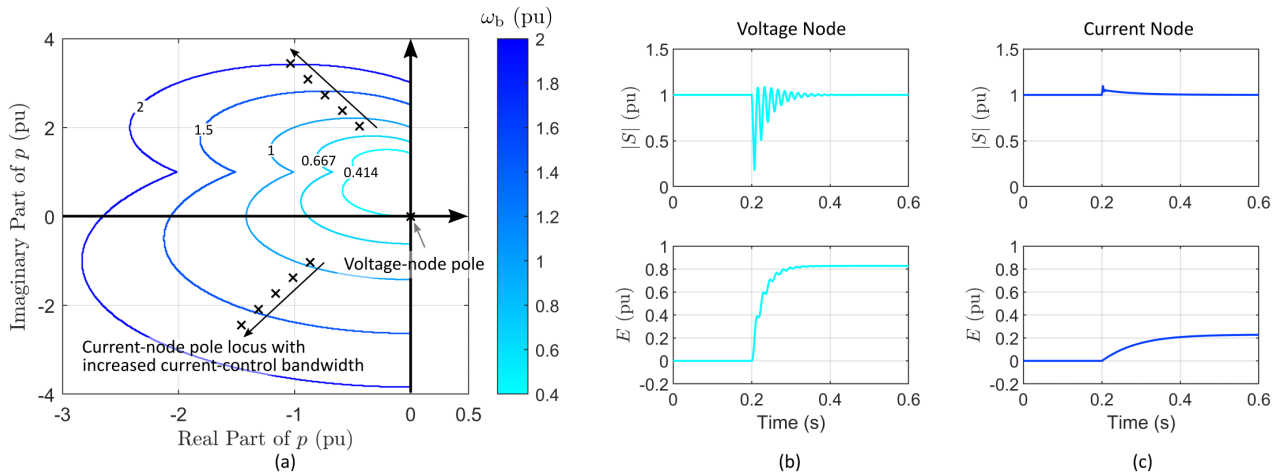

Fig. 4. Channel bandwidth and its impact on transient power. (a) Equi-bandwidth contours on the plane of channel pole indicating that current nodes have higher channel bandwidth ω_b than voltage nodes. (b)-(c) Transient power ($|S|$) and the accumulated energy (E) at a node subject to a phase jump at the remote end: (b) for a voltage node and (c) for a current node. The relatively low channel bandwidth associated with a voltage node results in high accumulated energy and requires a large energy cache. Variables in the figure are presented per unit.

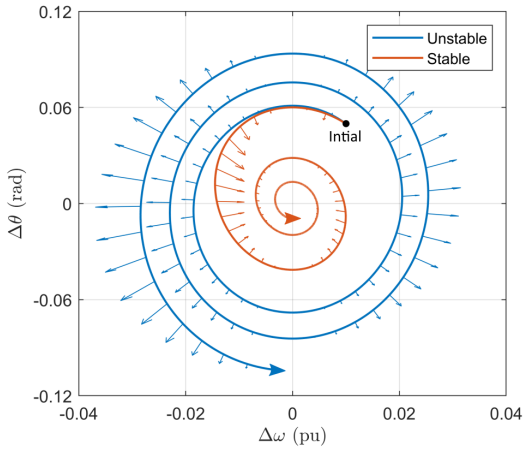

Fig. 5. Channel dynamics (dynamic frequency shift) may induce negative damping. The negative $\partial W/\partial\omega$ results in a vector field on the ω-θ phase plane pointing outward (shown as the outward arrow on the blue trajectory), which causes the trajectory to diverge from the equilibrium and makes the system unstable. This problem can be solved by injecting extra positive damping in frequency control, to make the vector field pointing inward (shown as the inward arrow on the amber trajectory) .

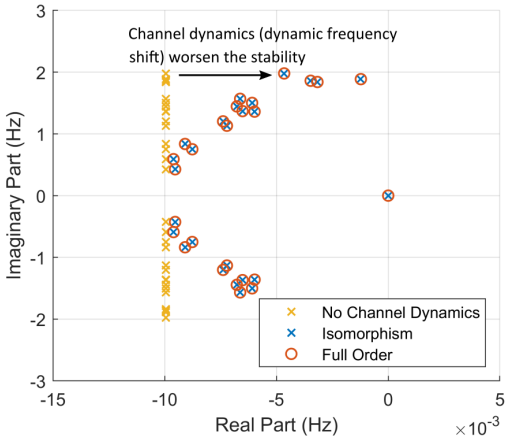

Fig. 6. Eigenvalues of IEEE 68-bus system consisting of 16 grid-forming converters with and without channel dynamics considered.

or without enough D_m, which validates the analysis. Additionally, Fig. 6 compares the eigenvalues of an IEEE 68-bus system consisting of 16 grid-forming converters (P-ω droop control or equivalently virtual-synchronous-generator control [6], [25]) modelled by different methods. When considering the channel dynamics by using the dynamic frequency shift and isomorphism model (blue cross), the system stability is almost same to the full-order model (red circle) and is worse than the simplified model without channel dynamics (yellow cross), which validates the accuracy of the proposed method. It is worth mentioning again that the channel includes all passive electrical elements (transmission lines, transformers, machine windings, and shunt/series compensators) as well as the virtual passive elements equivalent to the inner loops of grid-forming converters. This channel-induced negative damping illuminates the role of EMTs in phasor-domain analysis, which also agrees with the literature observing that the EMT dynamics tend to worsen the system stability [30].

C. Synchronizing Coefficient and Modulation-Demodulation

It is obvious that W_m in (16) depends on not only the frequency ω (given by the dynamic frequency shift), but also the phase angle θ (given by the modulation-demodulation). If considering the θ-induced dynamics only here and ignoring the previously-discussed ω-induced dynamics by setting $g_{mn} = G_{mn}(j\omega_0)$, in this case, we can re-write W_m in (16) as

$$\begin{aligned} W_m &= \mathrm{Re}\left(e^{-j\mu_m}\textstyle\sum_n G_{mn}A_mA_ne^{-j(\theta_m-\theta_n)}\right) \\ &= \textstyle\sum_n \Gamma_{mn}\sin(\theta_m-\theta_n+\gamma_{mn}) \end{aligned} \tag{17}$$

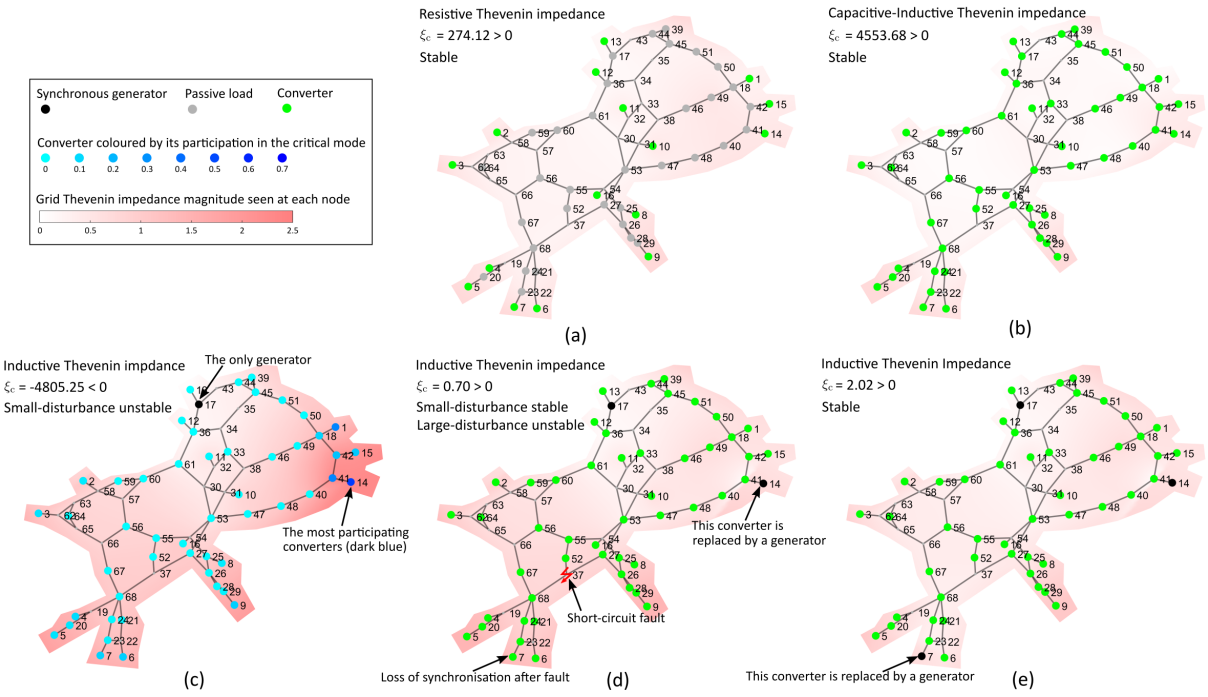

Fig. 7. Summary of test results on the IEEE 68-bus system with varying numbers of grid-following converters (green dots), synchronous generators (black dots) and passive loads (grey dots). Heat-map in shades of red indicates impedance magnitude seen at each node. The small-disturbance and large-disturbance stability of the tested system is marked via texts on the map, and the detailed transient responses are shown in Fig. 8. (a) 17 converters, 0 synchronous generators, with passive loads. (b) Converters at all 68 busses with active loads. (c) 1 synchronous generator (at node 17). (d) 2 synchronous generators (at nodes 14,17). (e) 3 synchronous generators (at nodes 7,14,17).

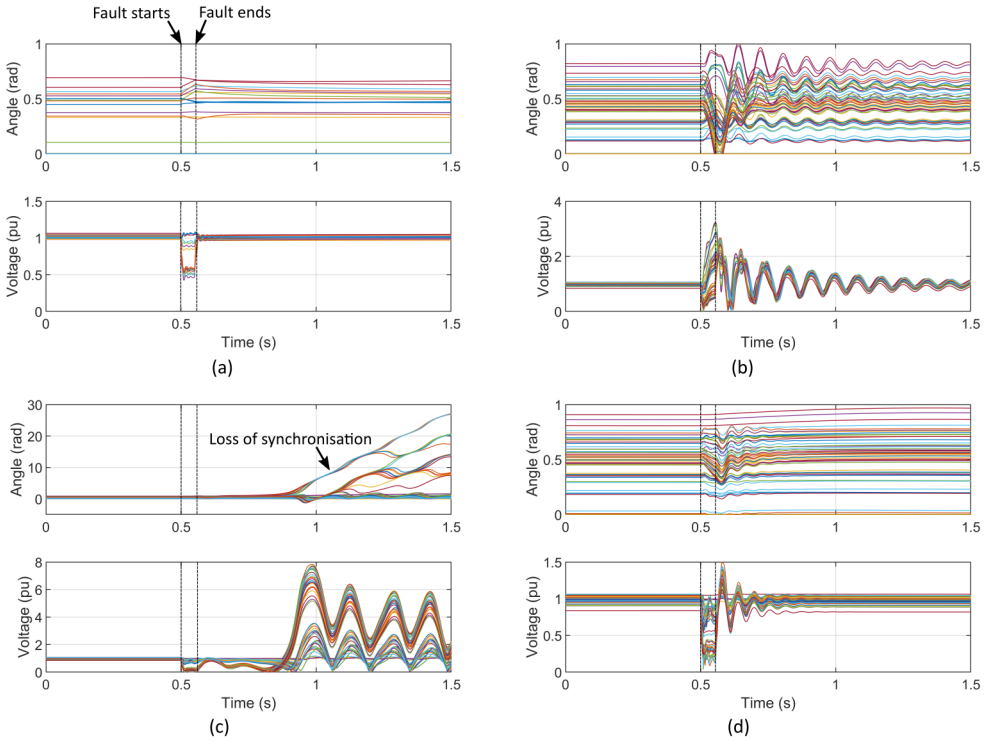

Fig. 8. Time-domain EMT simulations of the modified IEEE 68-bus system under a short-circuit fault, which occurs at bus 37 at 0.5 s and is cleared after 3 fundamental cycles, i.e., at 0.55 s. (a) 100% grid-following converters with passive loads. (b) 100% grid-following converters with active loads. (c) Two synchronous generators (at node 14,17). (d) Three synchronous generators (at node 7,14,17). The results in (a)-(d) corresponds to tests (a),(b),(d) and (e) in Fig. 7. The simulation result for test (c) is not stable around the equilibrium and is therefore not presented.

with

$$\begin{aligned}\Gamma_{mn} &= |G_{mn}A_mA_n| \\ \gamma_{mn} &= \pi/2 + \mu_m - \arg G_{mn}\end{aligned} \tag{18}$$

Γ_{mn} is the *generalized synchronizing coefficient*, and γ_{mn} is the offset angle. Equation (17) shows interesting properties. Γ_{mn} is symmetric ($\Gamma_{mn} = \Gamma_{nm}$) due to the reciprocity of electrical networks. The offset angle γ_{mn} is dependent on network topology as well as the projection angle μ_m for different apparatuses. In the following two conditions, γ_{mn} is approximately zero for $m \neq n$: (i) synchronization of grid-forming apparatuses via inductive transmission lines; and (ii) synchronization of grid-following converters via shunt resistances (passive loads). In such cases, the synchronization equation (15) is reduced to a second-order Kuramoto model which has a wide stability region [31]. This implies that grid-following converters could also have guaranteed stability that is similar to grid-forming apparatuses.

For cases where grid-forming and grid-following apparatuses co-exist, or where the power network is not purely inductive or resistive, $\gamma_{mn} \neq 0$, and the whole-system dynamic behaviour is more complicated. We can use linearization to evaluate the stability subject to small disturbances. Define $K_{mn} \triangleq \partial W_m/\partial\theta_n$ and $[K_H] \triangleq [H]^{-1}[K]$, $[K]$ is the matrix of K_{mn}, and $[H]$ is the diagonal matrix of H_m. $[K_H]$ is an extension of the synchronizing power coefficients in conventional power systems so that both voltage and current nodes can be considered [3]. The eigenvalue of $[K_H]$ determines the synchronizing capability of (15), and the eigenvector determines the modal participation [3]. We define the critical eigenvalue ξ_c as the non-zero eigenvalue of $[K_H]$ that has the minimum real part. The system is small-disturbance stable if ξ_c has a positive real part, as derived in Appendix E.

VI. Test of The IEEE 68-Bus Power System

A. Impacts of Grid-Forming and -Following on Stability

We verified our theoretic findings on the modified IEEE 68-bus system. The small-disturbance analysis results are summarized in Fig. 7. Fig. 8 illustrates the EMT simulation results. All parameters, scripts, models are available online [32]. We tested five cases with different proportions of grid-following converters, subject to small and large disturbances. Fig. 7(a)-(b) and Fig. 8(a)-(b) contain 100% grid-following converters with passive and active loads, and are stable under both small and large disturbances. We gradually replaced the converters by synchronous generators (grid-forming apparatuses) in Fig. 7(c)-(e), and found more complicated stability patterns. These agree well with the prediction of our theory. The critical eigenvalue ξ_c of $[K_H]$ provides accurate indication of small-disturbance stability in all cases. We also display in Fig. 7(c) the participation of each node in the critical eigenvalue, to show how $[K_H]$ helps to trace the origins of instability.

It is rather surprising to see that a power system with 100% grid-following converters is rather stable and re-synchronizes rather fast after faults, as shown in Fig. 7(a)-(b) and Fig. 8(a)-(b). It is also worth highlighting that the voltage at each bus node is also nearby 1 pu at steady-state, by properly setting the current reference of each grid-following converter based on the power flow analysis. It is even more surprising to see that adding one synchronous generator to the all-grid-following-converter network destabilizes the system, as shown in Fig. 7(c), which contradicts the conventional observation that synchronous generators are always helpful for grid stability. In this case, the current nodes dominate the power systems and the only voltage node follows the current nodes, which induces instability due to the asymmetry of synchronization [6]. This raises the importance of the reasonable placement of grid-forming apparatuses in a converter-dominated grid since grid-forming is not always helpful to stability. We use two techniques to guide this placement: participation analysis for the critical eigenvalue for small-disturbance stability, and observation of loss of synchronization via time-domain simulation for large-disturbance analysis. These techniques are effective as verified in Fig. 7(c)-(e) and Fig. 8(c)-(d), showing succeeding improvements of stability when synchronous generators are placed at the nodes identified most influential (14 and 7). Additionally, we shaded the grid map in Fig. 7 by the magnitude of the Thevenin impedance seen at each node. It is clear that small grid impedances tend to enhance stability, which agrees with traditional cognitive [3].

B. Operation of 100%-Grid-Following-Converter Grids

Since the results of the stability of grids with 100% grid-following converters are rather surprising, it is necessary to have more in-depth discussions.

Firstly, we modified the conventional v_q-PLL by introducing a droop feature in it. This helps to stabilize the frequency after fault with unbalance in net reactive power in the system, which is like a deliberate islanding of grid-following inverters.

Secondly, we need to emphasize that the stability of a 100%-grid-following system is very sensitive to the impedance of the network. The reason is that there are no explicit voltage sources in the system and all voltage control is implemented indirectly by changing currents to create voltages on the grid impedances. The sensitivity of voltage control against impedance implies reduced robustness in voltage stability. In a conventional system dominated by grid-forming, voltage control of a grid-following node is done by changing the reference of i_q, which is based on the assumption that the Thevenin impedance seen at the node is inductive. For a grid-following dominant system, this assumption no longer holds, as the behaviour of loads, which was clamped by grid-forming apparatuses, starts to manifest in the grid and changes grid impedances. For example, if loads are mainly resistive, the Thevenin impedance seen by a grid-following node is resistive and i_d instead of i_q should be used to regulate the voltage. On the other hand, i_d was usually used to control active power rather than voltage, which implies that the entire mechanism of voltage and power control needs to be tailor-made for a grid-following dominant grid, according to the nature of loads. This makes the issue of operating a 100% grid-following system much more complicated. In this article we focus on synchronization stability and illustrate the possibility of an all-grid-following system if only synchronization is of concern. That said, we need to acknowledge that this is a rather

simplified model and future work is needed to consolidate the feasibility in practice, especially when other outer loops (voltage and power) are included.

VII. Conclusions

The power-communication isomorphism theory reveals the intrinsic analogy of power systems and communication systems. This analogy (isomorphism) can be used to interpret the synchronization stability of power systems from a communication perspective. The power-based and signal-based synchronization schemes are unified into a common principle. The dynamic channel gain reveals the role of EMT dynamics in phasor-domain analysis. The channel bandwidth influences the speed of power transfer and angle synchronization. The channel-frequency dependency (dynamic frequency shift) could worsen the system damping. Additionally, the synchronization capability of multi-bus power systems is discussed. We demonstrate that a 100% grid-following-converter grid can be stabilized (in both small- and large-signal sense) without the existence of any voltage source. We also illustrate that adding only one grid-forming apparatuses into a 100% grid-following-converter grid could destabilize the system, but keep adding more grid-forming apparatuses can then enhance the system stability. The findings are verified on the modified IEEE 68-bus test system.

Appendix A
Duality Relationship of Synchronization

The active power P-based synchronization for grid-forming converters or synchronous generators is commonly adopted, which is equivalent to equation (3) with $\mu = 0$ and gives the generalized synchronizing power

$$W\,|_{\mu=0} = \mathrm{Re}(e^{-j0}\ S) = P \tag{19}$$

which is defined as *synchronizing active power*. By contrast, the synchronizing power for grid-following converters is a bit more complicated, as analyzed next. The PLL of a grid-following converter normally controls q-axis voltage, i.e.,

$$\mathrm{Re}(e^{-j\frac{\pi}{2}}\ A_v e^{j\theta_v}) = v_q \tag{20}$$

where $A_v e^{j\theta_v} = v_d + jv_q$ is the space vector of voltage, A_v is the voltage amplitude, and θ_v is the voltage phase angle. By noticing that

$$S = A_v e^{j\theta_v}\ (A_i e^{j\theta_i})^* = A_v A_i\ e^{j(\theta_v-\theta_i)} \tag{21}$$

where $A_i e^{j\theta_i} = i_d + ji_q$ is the space vector of current, A_i is the current amplitude, θ_i is the current phase angle, and $*$ is the complex conjugate operation. Based on (21), we can re-write (20) as

$$\frac{\mathrm{Re}(e^{-j(\frac{\pi}{2}-\theta_i)}\ S)}{A_i} = v_q \tag{22}$$

which further gives the generalized synchronizing power

$$W\,|_{\mu=\frac{\pi}{2}-\theta_i} = \mathrm{Re}(e^{-j(\frac{\pi}{2}-\theta_i)}\ S) = v_q A_i \propto v_q \tag{23}$$

For grid-following converters without reactive power generation, the q-axis current is simply zero at steady-state, which leads to an zero current phase angle of $\theta_i = 0$. In this case, (23) can be re-written as

$$W\,|_{\mu=\frac{\pi}{2}} = \mathrm{Re}(e^{-j\frac{\pi}{2}}\ S) = Q \tag{24}$$

which is defined as the *synchronizing reactive power*.

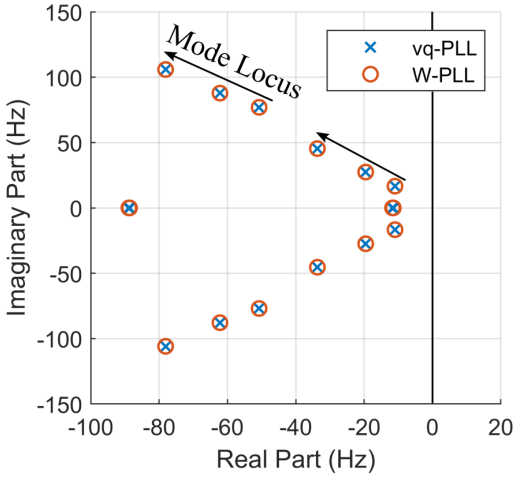

Fig. 9. Comparison of eigenvalues of v_q-PLL and W-PLL of a grid-following converter. The current control bandwidth is varying from around 50Hz to 100Hz.

The dynamics of W-PLL and v_q-PLL are compared next. Here, we investigate a grid-following converter with 100 Hz current control bandwidth, 10 Hz PLL bandwidth, and generating 0.5 pu active power and 0.1 pu reactive power to an infinite bus at rated conditions. It is worth mentioning that, the generalized synchronizing power W of W-PLL is calculated based on (23) and the controller gain of W-PLL is also scaled correspondingly, in order to achieve the same equivalent 10 Hz phase-locking bandwidth of W-PLL and v_q-PLL. Fig. 9 compares the eigenvalues of two PLL control methods with varying current control bandwidth from 50 Hz to 100 Hz. The eigenvalue locus of W-PLL (red circle) overlaps the eigenvalue locus of v_q-PLL (blue cross) in all cases, which indicate almost same small-signal stability. Fig. 10 shows the EMT simulation results of two different PLL configurations. A short-circuit fault occurs at 0.04 s and is cleared after three fundamental cycles. It is obvious that the waveform of W-PLL (dashed red line) overlaps the waveform of v_q-PLL (solid blue line), which indicates almost same transient stability. Both Fig. 9 and Fig. 10 valid the almost equivalent dynamics of v_q-PLL and W-PLL from the perspectives of both small-signal and transient.

Appendix B
Impedance Circuit Model of Power Converters

The impedance method is widely used to modeling and analyzing the output characteristics of power converters. It normally represents a converter as an impedance or admittance transfer function which captures the dynamic relationship between its terminal voltage and current [10], [11]. In [17], the impedance circuit model method is further proposed, which can visualize a closed-loop power converter as an impedance

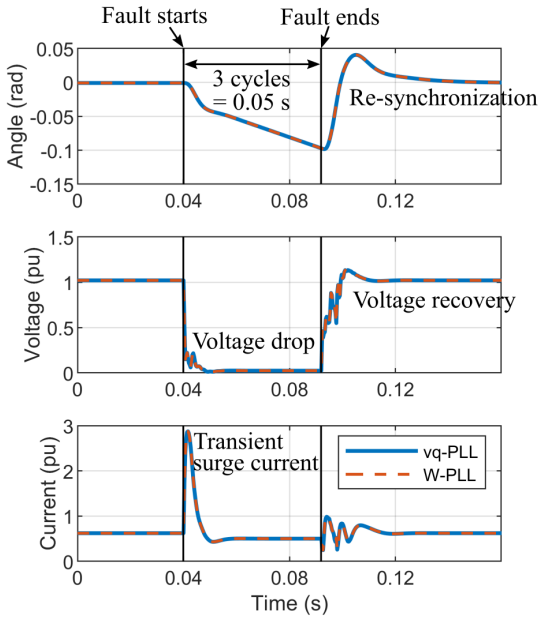

Fig. 10. Comparison of EMT simulation results of v_q-PLL and W-PLL of a grid-following converter. A short-circuit fault occurs at the middle point of the transmission line at 0.04 s and is cleared after three fundamental cycles.

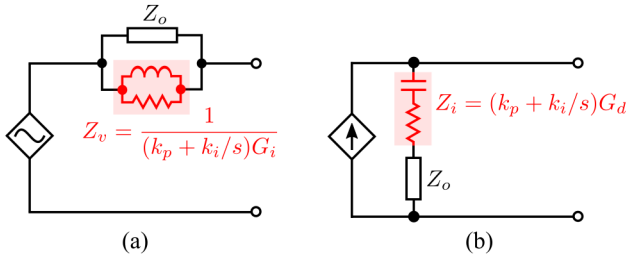

Fig. 11. Impedance circuit model of converters. (a) Grid-forming converter. (b) Grid-following converter.

circuit with discrete circuit elements. For example, as shown in Fig. 11, grid-forming and grid-following converters can be represented as Thevenin or Norton circuits with source impedances preserving the dynamics of internal controllers and ac-side filters. For a grid-forming converter, its output impedance is dominated by Z_v, i.e., the PI controller gains of its voltage control loop, which can be further physically interpreted as a virtual inductor and a virtual resistor in parallel [17]. By contrast, for a grid-following converter, its output impedance is dominated by Z_i, i.e., the PI controller gains of its current control loop, which can be further physically interpreted as a virtual capacitor and a virtual resistor in series [17]. Dynamics of other controllers and filters can also be accurately captured by Z_o [17], whose representation is omitted here.

After obtaining the impedance circuit models of converters, we can integrate these impedances into network lines. In this case, the dynamics of internal controllers and circuits of converters will also be integrated into the channel dynamics, so that we can only focus on the synchronization dynamics and simplify the analysis.

Appendix C
Derivation of Channel Bandwidth

The channel bandwidth equations (11)-(12) are obtained as follows. Applying angle perturbations at both ends of the channel g_{mn}, the corresponding complex power perturbation is

$$\Delta S_{mn} = S_{mn0} g_{mn0} (\Delta\vartheta_m^* + \Delta\vartheta_n + g_{mn0}^{-1} \Delta g_{mn}). \tag{25}$$

Linearising the channel gain equation (10) yields

$$d\Delta g/dt = (p - \varpi_0)\Delta g - g_0 \Delta\varpi \tag{26}$$

from which we get the transfer function from $\Delta\varpi$ to Δg

$$\Delta g(s) = -\frac{g_0}{s + \varpi_0 - p} \Delta\varpi(s). \tag{27}$$

Therefore,

$$g_{mn0}^{-1} \Delta g_{mn}(s) = \frac{-\Delta\varpi_n(s)}{s + \varpi_0 - p} = \frac{-s\Delta\vartheta_n(s)}{s + \varpi_0 - p}. \tag{28}$$

Putting this into (25) and noting that $\varpi_0 = j\omega_0$ (since the signal amplitude is constant in steady-state), we get the equations (11)-(12).

Appendix D
Calculation of Damping and Synchronizing Coefficients

The complex power from node n to node m is

$$S_{mn} = g_{mn} \underbrace{e^{\vartheta_n} e^{\vartheta_m^*}}_{\hat{S}_{mn}} \approx \underbrace{G_{mn}(\varpi_n)}_{f(\varpi)} \underbrace{e^{\vartheta_n} e^{\vartheta_m^*}}_{f(\vartheta)} \tag{29}$$

where $f(\varpi)$ contributes to the damping power, and $f(\vartheta)$ contributes to the synchronizing power. The total complex power at node m can be represented as

$$S_m = \sum_n S_{mn} = A_m^2 G_{mm} + e^{\vartheta_m^*} \sum_{n \neq m} G_{mn} e^{\vartheta_n} \tag{30}$$

For calculating damping coefficient, $\partial S_{mn}/\partial\varpi_n$ can be represented as

$$\frac{\partial S_{mn}}{\partial \varpi_n} = \frac{\partial G_{mn}(\varpi_n)}{\partial \varpi_n} e^{\vartheta_n} e^{\vartheta_m^*} = G'_{mn} e^{\vartheta_n} e^{\vartheta_m^*} \tag{31}$$

for both $n \neq m$ and $n = m$. Based on it, we can further get

$$\frac{\partial S_m}{\partial \omega_n} = \frac{\partial S_{mn}}{\partial \omega_n} = jG'_{mn} e^{\vartheta_n} e^{\vartheta_m^*} \tag{32}$$

for both $n \neq m$ and $n = m$.

For calculating the synchronizing coefficient, $\partial S_{mn}/\partial\vartheta_n$ can be represented as

$$\begin{aligned} \frac{\partial S_{mn}}{\partial \vartheta_n} &= G_{mn} e^{\vartheta_n} e^{\vartheta_m^*} = S_{mn0}, \text{ if } n \neq m \\ \frac{\partial S_{mm}}{\partial \vartheta_m} &= 0, \text{ if } n = m \end{aligned} \tag{33}$$

Based on it, we can further get

$$\begin{aligned} \frac{\partial S_m}{\partial \theta_n} &= \frac{\partial S_{mn}}{\partial \theta_n} = jG_{mn} e^{\vartheta_n} e^{\vartheta_m^*}, \text{ if } n \neq m \\ \frac{\partial S_m}{\partial \theta_m} &= -j \sum_{n \neq m} G_{mn} e^{\vartheta_n} e^{\vartheta_m^*}, \text{ if } n = m \end{aligned} \tag{34}$$

It is also worth mentioning that

$$\frac{\partial W}{\partial \omega} = \frac{\partial \mathrm{Re}(e^{-j\mu}S)}{\partial \omega} = \mathrm{Re}\Big(e^{-j\mu}\frac{\partial S}{\partial \omega}\Big) \tag{35}$$

The rule for $\partial W/\partial\theta$ is similar.

APPENDIX E
SMALL DISTURBANCE STABILITY OF SYNCHRONIZATION

Here, we show why the small-disturbance stability of the whole system is determined by the eigenvalues of $[K_H]$. Linearizing (15) yields

$$[\Delta\ddot{\theta}] = -[H]^{-1}[D][\Delta\dot{\theta}] - [K_H][\Delta\theta] \tag{36}$$

The generalized inertia and damping are usually proportional [3], so we have $[H]^{-1}[D] = \sigma[I]$ where $[I]$ is a unit matrix and $\sigma = D_m/H_m$. $[K_H]$ can be diagonalized by $[K_H] = [\Phi][\Xi][\Phi]^{-1}$ where $[\Xi]$ is a diagonal matrix containing the eigenvalues of $[K_H]$, and $[\Phi]$ contains the corresponding eigenvectors. Define the coordinate transformation $[\Phi]^{-1}[\Delta\theta] = [z]$, and transform (36) to the z coordinate

$$[\ddot{z}] = -\sigma[\dot{z}] - [\Xi][z]. \tag{37}$$

Since $[\Xi]$ is diagonal, (37) reduces to a series of decoupled second order systems

$$\ddot{z}_m = -\sigma\dot{z}_m - \xi_m z_m \tag{38}$$

where $m \in \{1, 2, \cdots, N\}$ and ξ_m is the m-th eigenvalue of K_H. The system (38) is stable if an only if its characteristic equation $s^2 + \sigma s + \xi_m = 0$ only has solutions in the left open half complex plane. We traverse s in the unstable right half plane to get the forbidden region of ξ_m, and the stable region is its complement

$$\text{Stable Region: } \{\xi_m \mid \mathrm{Re}\,\xi_m > \sigma^{-2}(\mathrm{Im}\,\xi_m)^2\}. \tag{39}$$

If sufficient damping is provided in synchronization control, σ is large enough to render $\sigma^{-2}(\mathrm{Im}\,\xi_m)^2$ very small, and the stability region is approximated by

$$\text{Stable Region: } \{\xi_m \mid \mathrm{Re}\,\xi_m > 0\}. \tag{40}$$

All ξ_m must be within the stable region to ensure the synchronization stability of the power system, with the only exception being the one that equals zero, which represents the collective spinning of the entire power system. Therefore we define the critical eigenvalue ξ_c as the non-zero ξ_m (eigenvalue of $[K_H]$) that has the minimum real part.

REFERENCES

[1] Y. Gu and T. C. Green, "Power system stability with a high penetration of inverter-based resources," *Proceedings of the IEEE*, 2022.

[2] J. Bialek, "What does the GB power outage on 9 august 2019 tell us about the current state of decarbonised power systems?" *Energy Policy*, vol. 146, p. 111821, 2020.

[3] P. Kundur, *Power system stability and control*. McGraw-hill New York, 1994, vol. 7.

[4] P. Kundur *et al.*, "Definition and classification of power system stability ieee/cigre joint task force on stability terms and definitions," *IEEE Trans. Power Syst.*, vol. 19, no. 3, pp. 1387–1401, 2004.

[5] J. Rocabert, A. Luna, F. Blaabjerg, and P. Rodríguez, "Control of power converters in AC microgrids," *IEEE Trans. Power Electron.*, vol. 27, no. 11, pp. 4734–4749, Nov. 2012.

[6] Y. Li, Y. Gu, and T. C. Green, "Revisiting grid-forming and grid-following inverters: A duality theory," *IEEE Transactions on Power Systems*, 2022.

[7] R. Rosso, X. Wang, M. Liserre, X. Lu, and S. Engelken, "Grid-forming converters: Control approaches, grid-synchronization, and future trends—a review," *IEEE Open Journal of Industry Applications*, vol. 2, pp. 93–109, 2021.

[8] J. Matevosyan, B. Badrzadeh, T. Prevost, E. Quitmann, D. Ramasubramanian, H. Urdal, S. Achilles, J. MacDowell, S. H. Huang, V. Vital *et al.*, "Grid-forming inverters: Are they the key for high renewable penetration?" *IEEE Power and Energy magazine*, vol. 17, no. 6, pp. 89–98, 2019.

[9] Y. Li, Y. Gu, and T. C. Green, "Interpreting frame transformations in ac systems as diagonalization of harmonic transfer functions," *IEEE Transactions on Circuits and Systems I: Regular Papers*, vol. 67, no. 7, pp. 2481–2491, 2020.

[10] L. Fan, Z. Miao, P. Koralewicz, S. Shah, and V. Gevorgian, "Identifying dq-domain admittance models of a 2.3-mva commercial grid-following inverter via frequency-domain and time-domain data," *IEEE Transactions on Energy Conversion*, vol. 36, no. 3, pp. 2463–2472, 2020.

[11] B. Wen, D. Boroyevich, R. Burgos, P. Mattavelli, and Z. Shen, "Analysis of dq small-signal impedance of grid-tied inverters," *IEEE Transactions on Power Electronics*, vol. 31, no. 1, pp. 675–687, 2015.

[12] Y. Xiong and Y. Ye, "Physical interpretations of grid voltage full feedforward for grid-tied inverter," *IEEE Transactions on Circuits and Systems II: Express Briefs*, vol. 66, no. 2, pp. 267–271, 2019.

[13] Z. Yao, Y. Zhang, and X. Hu, "Transformerless grid-connected pv inverter without common mode leakage current and shoot-through problems," *IEEE Transactions on Circuits and Systems II: Express Briefs*, vol. 67, no. 12, pp. 3257–3261, 2020.

[14] R.-J. Wai and W.-H. Wang, "Grid-connected photovoltaic generation system," *IEEE Transactions on Circuits and Systems I: Regular Papers*, vol. 55, no. 3, pp. 953–964, Apr. 2008.

[15] X. Wang, M. G. Taul, H. Wu, Y. Liao, F. Blaabjerg, and L. Harnefors, "Grid-synchronization stability of converter-based resources—an overview," *IEEE Open Journal of Industry Applications*, vol. 1, pp. 115–134, 2020.

[16] System Operability Framework, "Performance of Phase-locked Loop based converters," National Grid, Tech. Rep., 2018.

[17] Y. Li, Y. Gu, Y. Zhu, A. Junyent-Ferre, X. Xiang, and T. C. Green, "Impedance circuit model of grid-forming inverter: Visualizing control algorithms as circuit elements," *IEEE Trans. Power Electron.*, vol. 36, no. 3, pp. 3377–3395, Mar. 2021.

[18] L. Harnefors, "Modeling of three-phase dynamic systems using complex transfer functions and transfer matrices," *IEEE Trans. Ind. Electron.*, vol. 54, no. 4, pp. 2239–2248, Aug. 2007.

[19] F. Briz, M. W. Degner, and R. D. Lorenz, "Analysis and design of current regulators using complex vectors," *IEEE Transactions on Industry Applications*, vol. 36, no. 3, pp. 817–825, 2000.

[20] K. W. Martin, "Complex signal processing is not complex," *IEEE Transactions on Circuits and Systems I: Regular Papers*, vol. 51, no. 9, pp. 1823–1836, 2004.

[21] F. Milano, "Complex frequency," *IEEE Transactions on Power Systems*, vol. 37, no. 2, pp. 1230–1240, 2021.

[22] D. Pattabiraman, R. Lasseter, and T. Jahns, "Comparison of grid following and grid forming control for a high inverter penetration power system," in *2018 IEEE Power & Energy Society General Meeting (PESGM)*. IEEE, 2018, pp. 1–5.

[23] L. S. Czarnecki, "On some misinterpretations of the instantaneous reactive power pq theory," *IEEE transactions on power electronics*, vol. 19, no. 3, pp. 828–836, 2004.

[24] L. Zhang, L. Harnefors, and H.-P. Nee, "Power-synchronization control of grid-connected voltage-source converters," *IEEE Transactions on Power systems*, vol. 25, no. 2, pp. 809–820, 2009.

[25] S. D'Arco and J. A. Suul, "Equivalence of Virtual Synchronous Machines and Frequency-Droops for Converter-Based MicroGrids," *IEEE Transactions on Smart Grid*, vol. 5, no. 1, pp. 394–395, Jan 2014.

[26] S.-K. Chung, "A phase tracking system for three phase utility interface inverters," *IEEE Trans. Power Electron.*, vol. 15, no. 3, pp. 431–438, May 2000.

[27] W. K. Chen, *The electrical engineering handbook*. Elsevier, 2004.

[28] A. Oppeitheim, A. S. Willsky, and I. Young, "Signals and systems," *Prentice-Hall, Englewood Cliffs, New Jersey*, vol. 19, pp. 146–153, 1983.

[29] Y. Gu, Y. Li, Y. Zhu, and T. C. Green, "Impedance-based whole-system modeling for a composite grid via embedding of frame dynamics," *IEEE Transactions on Power Systems*, vol. 36, no. 1, pp. 336–345, 2020.

[30] Y. Li, Y. Gu, and T. Green, "Mapping of dynamics between mechanical and electrical ports in SG-IBR composite grids," *IEEE Transactions on Power Systems*, 2022.
[31] J. Peng, "Synchronization in the second-order kuramoto model," 2015.
[32] "Future Power Networks." [Online]. Available: https://github.com/Future-Power-Networks/Publications

Yitong Li (S'17-M'21) received the B.Eng degrees in electrical engineering from Huazhong University of Science and Technology, China, and the University of Birmingham, UK, in 2015. He received the M.Sc degree in future power networks and the Ph.D. degree in electrical engineering from Imperial College London, UK, in 2016 and 2021 respectively. He is currently an Associate Professor at Xi'an Jiaotong University, China. His current research interests include control of power electronic converters and analysis of power system dynamics.

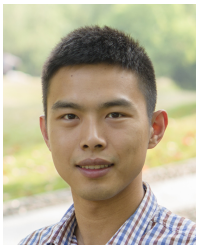

Yunjie Gu (M'18-SM'20) received the B.Sc. and the Ph.D. degree in Electrical Engineering from Zhejiang University, Hangzhou, China, in 2010 and 2015 respectively. He is now a Lecturer at Imperial College London, where he was an EPSRC-funded Innovation Fellow (award EP/S000909/1). Before his academic career, he was a Consulting Engineer at General Electric Global Research Centre, Shanghai, China. His research interests include stability theory for inverter-based power systems, stability-enhancing inverter technologies, and numerical methods for computer-aided stability analysis.

Timothy C. Green (M'89-SM'02-F'19) received a B.Sc. (Eng) (first class honours) from Imperial College London, UK in 1986 and a Ph.D. from Heriot-Watt University, Edinburgh, UK in 1990. He is a Professor of Electrical Power Engineering at Imperial College London. His research interest is in the control, stability and protection of power systems with very high penetration of inverter-based resources. Previously, in HVDC he has contributed converter designs that reduce losses while also providing control functions assist AC system integration. In distribution systems, he has pioneered the use of soft open points and the study of stability of microgrids. Prof. Green is a Chartered Engineering the UK and a Fellow of the Royal Academy of Engineering. He is also a fellow of the Chinese Society for Electrical Engineers.